2017 IEEE International Conference on Robotics and Automation (ICRA)
Singapore, May 29 - June 3, 2017

Magnetic Motion Control and Planning of Untethered Soft Grippers using Ultrasound Image Feedback

Stefano Scheggi, Krishna Kumar T. Chandrasekar, ChangKyu Yoon, Ben Sawaryn, Gert van de Steeg, David H. Gracias and Sarthak Misra

***Abstract*— Soft miniaturized untethered grippers can be used to manipulate and transport biological material in unstructured and tortuous environments. Previous studies on control of soft miniaturized grippers employed cameras and optical images as a feedback modality. However, the use of cameras might be unsuitable for localizing miniaturized agents that navigate within the human body. In this paper, we demonstrate the wireless magnetic motion control and planning of soft untethered grippers using feedback extracted from B-mode ultrasound images. Results show that our system employing ultrasound images can be used to control the miniaturized grippers with an average tracking error of 0.4±0.13 mm without payload and 0.36±0.05 mm when the agent performs a transportation task with a payload. The proposed ultrasound feedback magnetic control system demonstrates the ability to control miniaturized grippers in situations where visual feedback cannot be provided via cameras.**

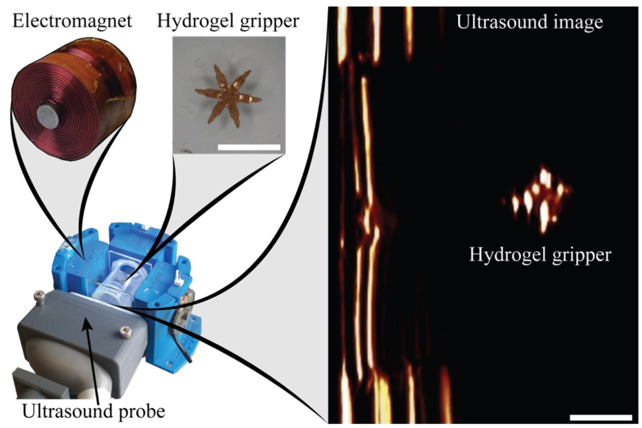

Fig. 1. The magnetic guidance system consists of three iron-core electromagnets fixed in a frame around a reservoir with the liquids. In order to fold/unfold the soft miniaturized grippers, a Peltier element is placed below the reservoir and used to regulate the temperature of the water wherein the grippers are floating. The position of the gripper is determined using an ultrasound probe 18L6HD (Siemens ACUSON S2000, Siemens Healthcare, Mountain View, USA). Magnetic forces are exerted on the gripper to control its position. The scale bar is 4 mm.

I. Introduction

Miniaturized agents with grasping capabilities provide significant advantages in achieving complex tasks like precise micro-assembly, minimally invasive surgery, cell manipulation, and lab-on-a-chip applications [1]–[7]. Recent studies have demonstrated tracking, closed-loop control and the ability of the grippers to pick-and-place biological material in dynamic environments [8]–[10]. These experiments used optical images acquired by a camera. However, the use of cameras might be unsuitable for localizing miniaturized agents in medical or surgical applications within the human body.

Previous studies used Magnetic Resonance Imaging (MRI) to image and control magnetic drug carriers, nanorobots, and magnetotactic bacteria [11], [12]. However, a major disadvantage in using an MR system for tracking and actuation is the possibility of a time-delay due to communications between the various modules of the interventional platform. This time-delay could cause instability in the closed-loop control system and possibly limit the realization of the control method in real-time. Different from MRI, ultrasound (US) has high frame rates that allows for the realization of real-time control, and is compatible with clinical interventions [13]. Moreover, US scanning is more easily accessible than MRI. It allows dynamic visualization with direct interaction between the clinician and the patient, as well as allowing guided intervention to be performed at the same time. Related studies on US used a high-frequency scanner to evaluate the motion of superparamagnetic iron oxide nanoparticles [14], [15]. The closed-loop position control of paramagnetic microparticles under US guidance has been previously reported in [16]. In addition, Sanchez *et al.* demonstrated the use of US feedback to track and control self-propelled, fast-moving microrobots [17].

In this study, we demonstrate an integrated system that localizes and controls soft miniaturized grippers to safely reach a target using US images (Fig. 1). This offers the potential to use untethered grippers to autonomously perform advanced manipulation and transportation tasks in clinically relevant scenarios. The system consists of a US tracker which localizes the position of the grippers. A Proportional-Integral-Derivative (PID) magnetic control scheme is used

S. Scheggi, Krishna Kumar T. Chandrasekar, B. Sawaryn, G. van de Steeg, and S. Misra are affiliated with the Surgical Robotics Laboratory, Department of Biomechanical Engineering, MIRA - Institute for Biomedical Technology and Technical Medicine, University of Twente, 7522 NB, The Netherlands. S. Misra is also affiliated with the Department of Biomedical Engineering, University of Groningen and University Medical Center Groningen, 9713 GZ, The Netherlands.

C. Yoon and D.H. Gracias are with the Department of Materials Science and Engineering, The Johns Hopkins University, MD 21218, USA. D.H. Gracias is also affiliated with the Department of Chemical and Biomolecular Engineering, The Johns Hopkins University, MD 21218, USA.

The research leading to these results has received funding from the Netherlands Organization for Scientific Research (NWO) Innovative Medical Devices Initiative (IMDI) - Project: USE (Ultrasound Enhancement) and from the European Union's Horizon 2020 Research and Innovation Programme - Project: ROBOTAR (Grant Agreement #638428). We also acknowledge funding from the US National Institutes of Health (NIH) under award number RO1EB017742. The content is solely the responsibility of the authors and does not necessarily represent the official views of the NIH.

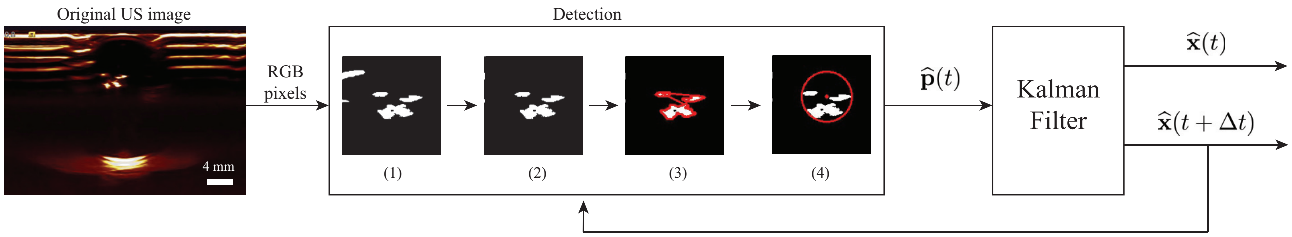

Fig. 2. Flowchart depicting the tracking process. From left to right, a B-mode image is taken from the ultrasound (US) machine. In the detection phase, we consider only the Red channel of the image. (1) A threshold on the Red channel is employed in order to properly detect the gripper. (2) Blobs which are too small or too far from the previous position of the gripper are discarded, while the remaining blobs are merged and kept for further consideration. (3) The contours of the segmented area are computed. (4) A circle fitting is applied on such contours in order to detect the pose $\widehat{\mathbf{p}}(t)$ of the gripper. Finally, a Kalman filter is used to estimate the state $\widehat{\mathbf{x}}(t)$ of the gripper, as well as a one-step ahead prediction of it $\widehat{\mathbf{x}}(t+\Delta t)$, being Δt the sampling time of the system. The predicted state of the gripper is used in the next frame to speed up the detection procedure.

to pull the grippers towards the reference position. By using the Linear Quadratic Gaussian Motion Planner (LQG-MP), we show that tracking and motion errors of the gripper can be taken into account during the planning phase, and proper obstacle-free paths can be computed in order to avoid collisions with the environment, e.g., sensitive organs or tissues. Finally, by combining magnetic and temperature control, we demonstrate the capability of soft miniaturized grippers to manipulate a spherical bead and transport it to a target area. To the best of our knowledge, our results represent the first experimental demonstration of the use of a magnetic system coupled with a US probe that simultaneously, (1) detects and tracks miniaturized untethered grippers using US images, (2) successfully controls the grippers along paths performing manipulation and transportation tasks, and (3) robustly controls the grippers along obstacle-free motion plans by taking into account tracking errors and the motion uncertainty of the grippers.

The remainder of this paper is organized as follows: Section II describes the technique used to detect the grippers. Section III shows the electromagnetic system and the control policy. Section IV presents and discusses the experimental results. Finally, Section V concludes and provides directions for future work.

II. Tracking of the soft miniaturized untethered grippers

In order to perform precise and robust motion control in unstructured environments, an image-guided tracking algorithm is necessary. In what follows, we describe the algorithm used to estimate the pose of the gripper from US images. The US images are acquired using a Siemens 18L6HD transducer (Siemens ACUSON S2000, Siemens Healthcare, Mountain View, USA) operating with a frequency of 16 MHz with an in-plane resolution of approximately 0.09 mm per pixel. Then, we report an extensive validation of the proposed approach, and a comparison with results obtained using a microscopic camera. Let $\mathbf{p}(t) = [x(t),\ y(t)]^T \in \mathbb{R}^{2\times 1}$ be the position of a gripper in 2D space at time t and $\mathbf{v}(t) = [v_x(t),\ v_y(t)]^T \in \mathbb{R}^{2\times 1}$ its velocity. The state of the gripper is defined as $\mathbf{x}(t) = [\mathbf{p}(t),\ \mathbf{v}(t)] \in \mathbb{R}^{4\times 1}$. Let us consider the miniaturized gripper as a second order system controlled by applying suitable force inputs. The tracking algorithm estimates the state $\widehat{\mathbf{x}}(t)$ of the gripper at runtime (Fig. 2).

In the initial phase, it estimates the position $\widehat{\mathbf{p}}(t) = [\hat{x}(t),\ \hat{y}(t)]^T$ of the gripper. Then, a standard Kalman filter is used to compute the estimated state $\widehat{\mathbf{x}}(t)$ from position estimates $\widehat{\mathbf{p}}(t)$. The Kalman filter provides an estimation of the current state $\widehat{\mathbf{x}}(t)$ as well as a one-step ahead prediction of it $\widehat{\mathbf{x}}(t+\Delta t)$, assuming a constant sampling time Δt of the system. The process and measurement noises are obtained from zero mean multivariate Gaussian distributions $N(\mathbf{0}, \mathbf{Q})$ and $N(\mathbf{0}, \mathbf{R})$, respectively, where $\mathbf{Q} \in \mathbb{R}^{4\times 4}$ and $\mathbf{R} \in \mathbb{R}^{2\times 2}$ are the empirically determined covariance matrices. In order to speed up the detection procedure, temporal continuity is exploited to track the grippers in a sequence of frames. Given the predicted state $\widehat{\mathbf{x}}(t+\Delta t)$ of the tracked gripper at time t, in the next frame the image pixels that are within a preset range from that estimation are kept, whereas the remaining pixels are discarded.

The proposed method is evaluated on three different datasets of more than 4000 images. The datasets report the common motion of the miniaturized grippers during manipulation and transportation tasks (Fig. 3). In order to generate ground truth data for the evaluation of the tracker, all the frames are manually labeled. This is a common approach in the relevant literature, since accurate ground truth data for such agents are hard to obtain [18], [19]. The evaluation shows a tracking error of 0.51 ± 0.33 mm, 0.49 ± 0.26 mm, and 0.26 ± 0.13 mm, for the three sequences, respectively. The tracking errors correspond to ∼12.75 %, ∼12.25 %, and ∼6.5 % of the body length of the miniaturized gripper. By comparing the proposed tracker with the one developed by Pacchierotti *et al.* for CCD cameras, we observe that the US tracker is less accurate [20]. In fact, by using microscopic cameras images, the average tracking error is about 106 μm (∼2.5 % of the body length). This is mainly due to the lower resolution of the US images (∼8 times worse than CCD images), and the presence of artifacts and occlusions. The proposed tracker can run at an average frame rate of 100 frame per second on a PC that has an Intel Xeon CPU 3.2 GHz processor and 8 GB of RAM.

III. Modeling of the US-based magnetic system

Wireless control of the soft miniaturized untethered grippers is accomplished using an array of iron-core electromagnets and an US system. The US probe (Siemens ACUSON S2000, Siemens Healthcare, Mountain View, USA) is placed

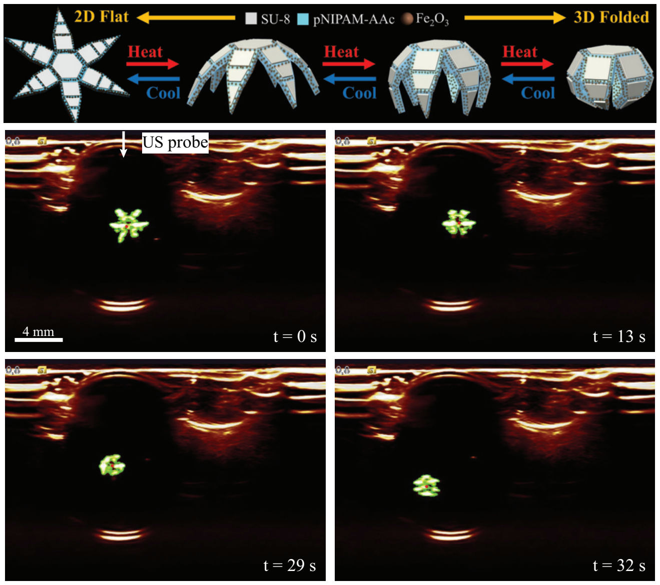

Fig. 3. Representative snapshots from the tracking experiment (best viewed in color). *Top*: Schematic of a representative folding and unfolding experiment. *Middle and bottom*: In the third video sequence (2229 frames), the miniaturized gripper moves downward and folds simulating a grasping task. For each snapshot, the estimated configuration of the gripper is displayed in green. *Please refer to the accompanying video that shows the results of the tracking experiments.*

at about 20 mm from the center of the workspace of our magnetic system. The workspace is 40×25 mm^2, as shown in Fig. 1. The magnetic system consists of three iron-core electromagnets. Each electromagnet is powered by an Elmo Whistle 1/60 servo controller (Elmo Motion Control, Petach-Tikva, Israel).

The magnetic force $\mathbf{F}(\mathbf{p}) \in \mathbb{R}^{2\times1}$ on a gripper positioned at $\mathbf{p} \in \mathbb{R}^{2\times1}$ is given by

$$\mathbf{F}(\mathbf{p}) = \nabla(\mathbf{m}_g \cdot \mathbf{B}(\mathbf{p})), \quad (1)$$

where $\mathbf{m}_g \in \mathbb{R}^{2\times1}$ and $\mathbf{B}(\mathbf{p}) \in \mathbb{R}^{2\times1}$ are the magnetic dipole moment of the gripper and the induced magnetic field, respectively [21], [22]. Since there is no electrical current and no displacement current flowing through the region occupied by the agent, the curl of the magnetic field $\mathbf{B}(\mathbf{p})$ is zero. Moreover, since the iron cores of the electromagnets used in our setup are not saturated, (1) can be rewritten as,

$$\mathbf{F}(\mathbf{p}) = (\mathbf{m}_g \cdot \nabla)\widetilde{\mathbf{B}}(\mathbf{p})\mathbf{I} = \Lambda(\mathbf{m}_g, \mathbf{p})\mathbf{I}, \quad (2)$$

where $\mathbf{I} \in \mathbb{R}^{3\times1}$, $\widetilde{\mathbf{B}}(\mathbf{p}) \in \mathbb{R}^{3\times3}$, and $\Lambda(\mathbf{m}_g, \mathbf{p}) \in \mathbb{R}^{2\times3}$ are the input current vector, a matrix that maps currents into magnetic fields, and a matrix that maps currents into magnetic forces, respectively [23]. The map $\Lambda(\cdot)$ is calculated by the superposition of the contribution of each of the electromagnets based on the linearity of the magnetic field and current. In order to determine $\Lambda(\cdot)$ it is necessary to compute both $\mathbf{m}_g$ and $\mathbf{B}(\mathbf{p})$. The magnitude of $\mathbf{m}_g$ was determined using the *U-turn* technique [8]. The induced magnetic field $\mathbf{B}(\mathbf{p})$ was evaluated in previous studies using a finite element analysis, and successively verified using a 3-axis 3MH3 Teslameter (SENIS AG, Baar, Switzerland) mounted on the end-effector of an XYZ Cartesian robot [24].

The magnetic force-current map is used in the implementation of a closed-loop control system of the soft miniaturized untethered grippers based on feedback obtained by an US device.

In order to fold/unfold the soft miniaturized grippers, we regulate the temperature of the water wherein the grippers are floating using a Peltier element (Fig. 4). The range of temperatures used to fold/unfold the soft miniaturized grippers is between 24° C and 27° C [8]. The Peltier element is placed below the reservoir of water. A closed-loop control is used to regulate the temperature of the Peltier element using the values of water temperature provided by a thermometric probe.

IV. Experimental validation

In this section, we report three different experiments in order to show the possibility for the soft miniaturized grippers to: (1) follow a pre-defined path, (2) autonomously move in a cluttered environment, and (3) firmly grasp an object and transport it to a target area; *please refer to the accompanying video for the visualization of the experiments*. The soft miniaturized grippers used in this work are composed of a stiff SU-8 and thermally responsive pNIPAM-AAc segmented bilayer (Fig. 4). The grippers open and close reversibly due to a lower critical solution temperature (LCST) phase transition and associated swelling or shrinkage in the pNIPAM-AAc layer in response to temperature changes. In order to make the grippers responsive to magnetic fields, the pNIPAM-AAc layer is doped with 3 % (w/w) Fe_2O_3 magnetic nanoparticles. When fully opened, the grippers have an hexagram shape with a tip-to-tip distance of 4 mm. When fully closed, the grippers have the shape of a sphere with a 0.4 mm radius. More details of the fabrication and mechanics modeling of the grippers are described in a previous publication [25].

A. Motion control

In the first scenario, we demonstrate that soft miniaturized untethered grippers can be controlled using US images to follow a pre-defined path. The magnetic force at time instant t is regulated using a PID controller,

$$\mathbf{F}(\mathbf{p}(t)) = \mathbf{K}_p(\mathbf{r}(t) - \widehat{\mathbf{p}}(t)) + \mathbf{K}_i \int_0^t (\mathbf{r}(\tau) - \widehat{\mathbf{p}}(\tau))d\tau + \mathbf{K}_d(\dot{\mathbf{r}}(t) - \widehat{\mathbf{v}}(t)), \quad (3)$$

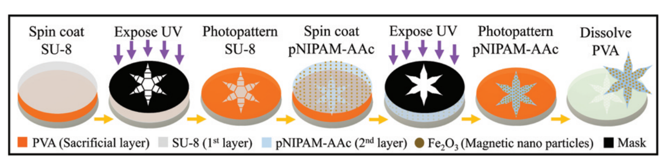

Fig. 4. Schematic showing the segmented, bilayer miniaturized untethered gripper composed of a stiff, segmented, SU-8 polymer coupled with a 3 % (w/w) magnetic nanoparticle (Fe_2O_3) doped thermally stimuli responsive poly(N-isopropylacrylamide-co-acrylic acid) (pNIPAM- AAc) layer.

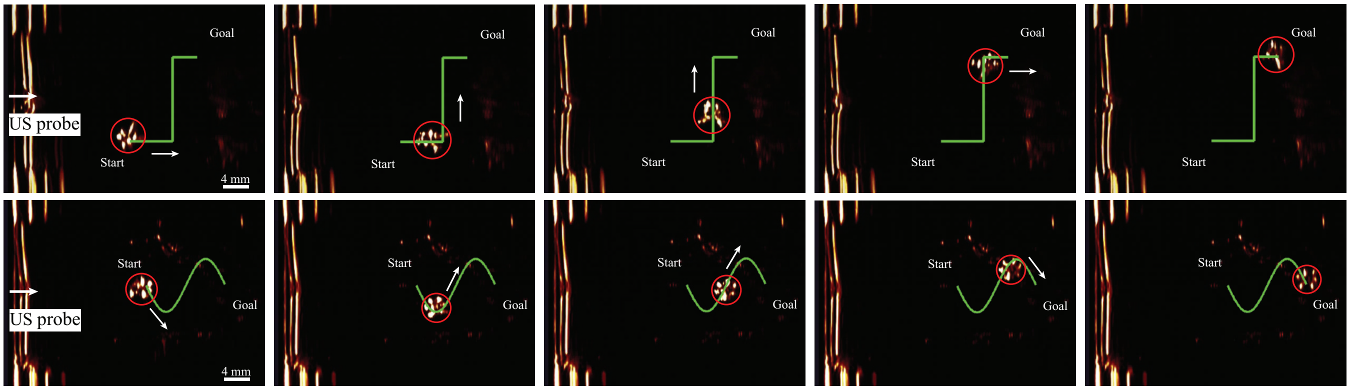

Fig. 5. Magnetic closed-loop motion control of a soft miniaturized gripper using US feedback: (*Top*) step path; (*bottom*) sinusoidal path. The gripper moves along the green path under the influence of the magnetic field gradients generated using a Proportional-Integral-Derivative controller coupled with the force-current map (2). The diameter of the gripper is approximately 4 mm. *Please refer to the accompanying video that demonstrates the path following control of a soft miniaturized gripper using US feedback.*

where $\mathbf{K}_p \in \mathbb{R}^{2\times2}$, $\mathbf{K}_i \in \mathbb{R}^{2\times2}$, and $\mathbf{K}_d \in \mathbb{R}^{2\times2}$ are the controller positive-definite gain matrices. Moreover, $\mathbf{r}(t) \in \mathbb{R}^{2\times1}$, $\dot{\mathbf{r}}(t) \in \mathbb{R}^{2\times1}$ are the reference position and its time derivative, while $\widehat{\mathbf{p}}(t) \in \mathbb{R}^{2\times1}$, $\widehat{\mathbf{v}}(t) \in \mathbb{R}^{2\times1}$ are the estimated position and velocity of the gripper (cf. Sect. II). The desired force $\mathbf{F}(\mathbf{p})$ is mapped into the currents $\mathbf{I}$ using (2).

Two different paths are used: a step path and a sinusoidal path (Figs. 5-6). Motion control using US feedback is achieved by providing way-points to the control system. The experiment is repeated ten times. We observe that the controlled grippers follow the step trajectory at an average speed of 0.35 ± 0.13 mm/s. For the sinusoidal path, the average speed of the grippers is 0.41 ± 0.14 mm/s. The average positioning error for the step and the sinusoidal path is 0.32 ± 0.09 mm and 0.48 ± 0.1 mm ($\sim$8 % and $\sim$12 % of the body length of the miniaturized gripper), as shown in Fig. 6. In order to show the validity of the proposed approach, we compare these results with prior results where a microscopic camera was used to image the untethered soft grippers [8]. Previously, we reported an average positioning error of $\sim$3 % of the body length of the gripper [8]. As described in Section II, the higher positioning error of the proposed system relies in the lower resolution and acquisition time of the US images, and in the presence of artifacts and occlusions.

B. Motion planning with uncertainty

Results presented in Sect. IV-A show that motion uncertainty, e.g. due to un-modeled external influences on the motion of the soft miniaturized gripper, and imperfect state information due to partial or noisy estimations of the gripper's state, generate positioning errors. Because safety and accuracy are of critical importance for many medical applications such as targeted drug delivery or biopsies, these uncertainties will have significant influence on determining which path is the best for the task at hand.

In this section, we adapt the Linear Quadratic Gaussian Motion Planner (LQG-MP) to generate a motion plan which minimizes the probability of collisions between the gripper and the environment [26]. LQG-MP is based on the Linear Quadratic Controller (LQG-controller) with Gaussian models of the motion and sensing uncertainty. For the given stochastic model of the gripper dynamics and of the sensor measurements (cf. Sect. II), it is possible to compute in advance (i.e., before execution) the *a-priori* probability distributions of the states and the control inputs of the agent along a given path. These distributions can be used to compute the probability that collisions will be avoided by the soft miniaturized gripper [27].

We use a sampling-based Rapidly-exploring Random Tree (RRT) planner to generate a set of $N \in \mathbb{R}_{>0}$ obstacle-free motion plans $\Gamma = \{\gamma^i, i = 1, \ldots, N\}$ [28]. Each entry of the motion plan γ^i represents a control input $\mathbf{F}(\mathbf{p})$ that is applied to the agent after every time interval Δt. The final plan γ^{best} is selected using the LQG-MP by minimizing the probability of collision with the obstacles (Algorithm 1). The planner is customized for the motion planning of soft miniaturized grippers. It is executed offline before starting each experiment, and runs for approximately 3 seconds, generating and evaluating an average of 30 successful motion plans. The experiment is repeated ten times. Among all the trials, the average probability of success of the paths selected using the LQG-MP is 94 %. In all the trials the grippers safely reached the target area, avoiding all the obstacles

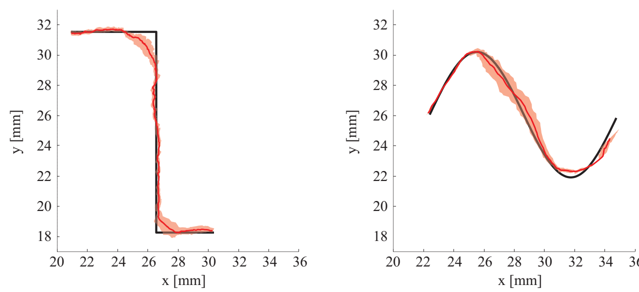

Fig. 6. Motion control of soft miniaturized grippers based on the feedback provided by an US system: (*Left*) step path; (*right*) sinusoidal path. The black line represents the reference path, the red line shows the average path of the miniaturized grippers, and the red shaded area represents the standard deviation for the corresponding point among all the performed trials. The average positioning error for the step and the sinusoidal path is 0.32 ± 0.09 mm and 0.48 ± 0.1 mm, respectively.

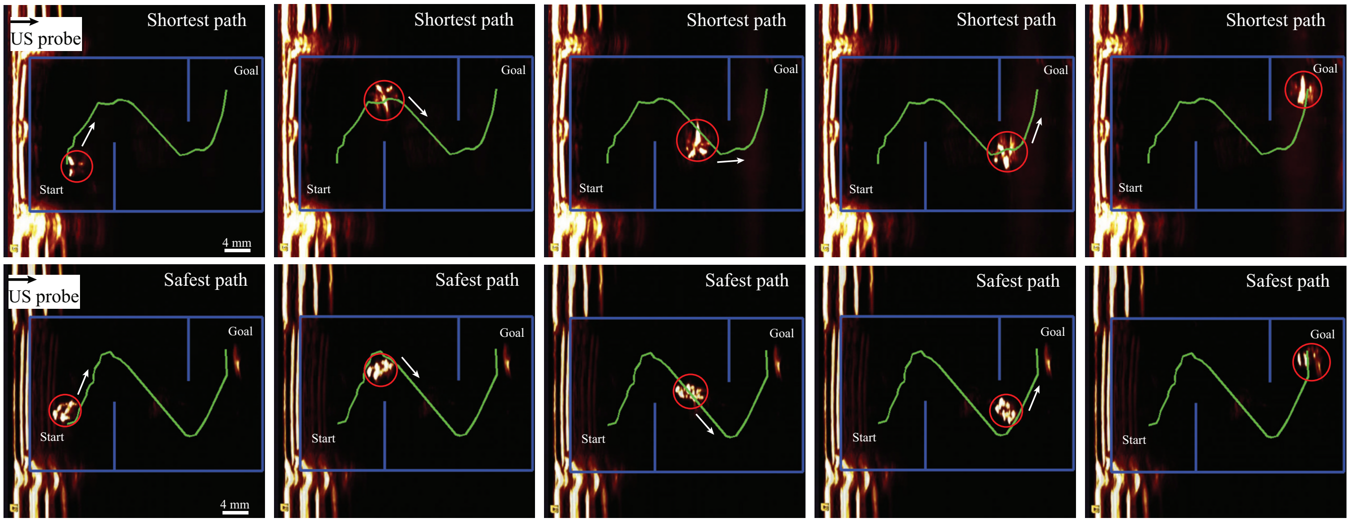

Fig. 7. Representative snapshots of the motion planning experiments. The soft miniaturized untethered gripper moves from the initial position toward a target area in a cluttered environment. The virtual obstacles (walls) are shown in blue. The planned obstacle-free trajectory is represented as a green line and it is computed offline (preoperative planning). A Linear Quadratic Gaussian Motion Planner computes a set of obstacle-free trajectories. *Top*: Among all the computed trajectories, the shortest one is selected. *Bottom*: The safest path, which minimizes the probability of collision with the environment, is selected. *Please refer to the accompanying video for the visualization of this experiment.*

present in the environment. Fig. 7 depicts the shortest path (top) and the safest one (bottom) selected using the LQG-MP.

C. Pick-and-place

In the last experimental scenario, we show the ability of the soft miniaturized untethered grippers to grasp a 0.5 mm polyester spherical bead weighing 0.6±0.1 mg, and transport it along a path, until a target area is reached (Fig. 8). This task was chosen in order to resemble real surgical interventions such as deployment of a vascular implant or biopsies [29]. A gripper is positioned in the starting position and it has to reach the bead. The control law (3) proposed in Sect. IV-A is used to move the gripper. Once the bead is reached, the temperature is increased using the Peltier element until the gripper folds and grasps the bead (cf. Sect. III). Therefore, the bead is captured within the soft gripper and can be dragged to the desired target location along a pre-defined path. The experiment is repeated ten times with an average tracking error of 0.36 ± 0.05 mm ($\sim$9 $\%$ of the body length of the miniaturized gripper). The bead is transported for a distance of 14.5 mm with an average velocity of 0.39 ± 0.06 mm/s.

Algorithm 1 Given a fixed planning time T and a target area $\mathbf{p}_{target}$, we use the Rapidly-exploring Random Tree (RRT) planner to generate a set of obstacle-free motion plans Γ. Each motion plan γ consists in a sequence of control inputs that should be applied to the agent after every time interval Δt. The final plan γ^{best} is computed using the LQG-MP approach by minimizing the probability of collision.

$\Gamma \leftarrow \emptyset$;
while computation_time() $< T$ **do**
  $\gamma \leftarrow$ RRT($\widehat{\mathbf{x}}$, $\mathbf{p}_{target}$, Δt);
  $\Gamma \leftarrow$ ADD(γ);
end while
$\gamma^{best} \leftarrow$ LQG-MP(Γ);

V. Conclusions and Future Work

In this paper, we demonstrate the tracking, wireless magnetic motion control, and motion planning of soft miniaturized untethered grippers using US feedback. Despite the inevitable motion artifacts obtained in the US images, the grippers are controlled along a path at an average position tracking error of 0.4±0.13 mm without payload. By using a Linear Quadratic Gaussian Motion Planner, we show that obstacle-free paths for the grippers can be computed by taking into account motion errors and imperfect state estimations. Finally, we demonstrate the possibility to pick and move 0.5 mm beads. Manipulation and transportation tasks are completed with an average position tracking error of 0.36 ± 0.05 mm.

As a part of future work, we plan to control the soft miniaturized untethered grippers in 3D space using ultra-fast US images that sweep the spaces, or specialized 3D US probes optimized to acquire/render images in real-time. Moreover, we will consider the use of high-intensity focused US to change the temperature locally and perform manipulation tasks *in-vivo*. Furthermore, motion control and planning of soft miniaturized grippers will be achieved in fluidic micro-channels with time-varying flow rates based on the feedback provided by the US system to enable eventual applicability *in-vivo*.

References

[1] N. Dechev, W. L. Cleghorn, and J. K. Mills. Microassembly of 3-d microstructures using a compliant, passive microgripper. *J. of Microelectromechanical Systems*, 13(2):176–189, 2004.

[2] T. Yoneyama, T. Watanabe, H. Kagawa, J. Hamada, Y. Hayashi, and M. Nakada. Force detecting gripper and flexible micro manipulator for neurosurgery. In *Proc. IEEE Int. Conf. on Engineering in Medicine and Biology Society*, pages 6695–6699, 2011.

[3] A. Ichikawa, S. Sakuma, F. Arai, and S. Akagi. Untethered micro-robot with gripping mechanism for on-chip cell surgery utilizing outer magnetic force. In *Proc. IEEE Int. Conf. on Robotics and Automation*, pages 3795–3800, 2014.

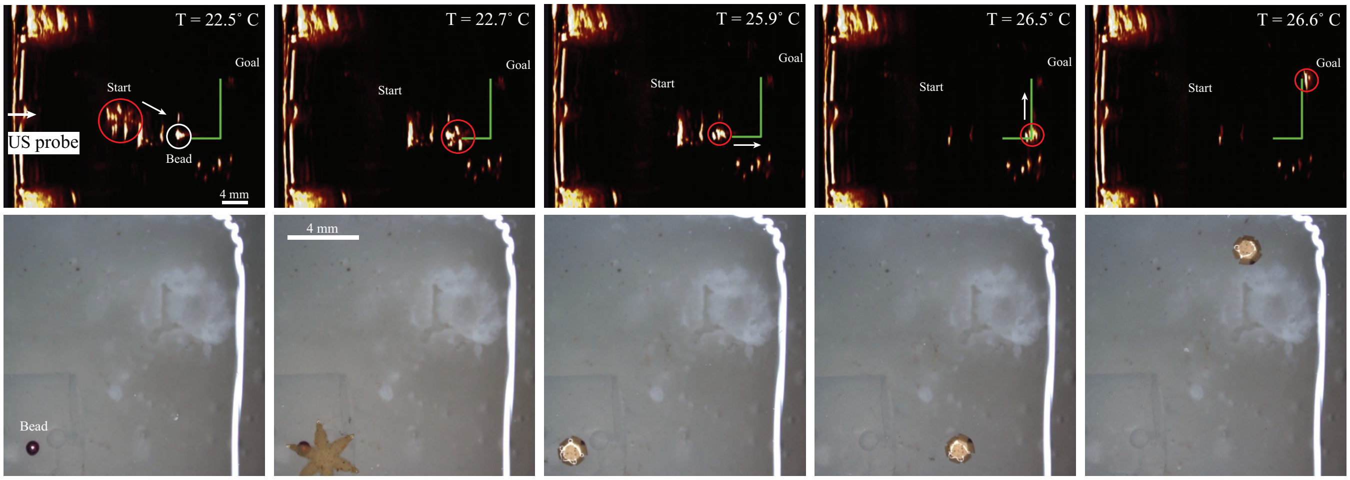

Fig. 8. Representative snapshots of the soft miniaturized gripper during manipulation and transportation of a 0.5 mm bead. The gripper moves from an initial position toward the bead. Once the target is reached, the temperature is increased until the system classifies the gripper as closed. A pre-defined trajectory then guides the gripper to the target area. Temperatures (T) are shown on the top-right corner of each snapshot. *Top*: Snapshots acquired using an US probe. *Bottom*: In order to facilitate the reader's understanding of this experiment, we provided the snapshots acquired with a microscopic camera. Please note that the magnetic controller uses only the feedback provided by the US probe. *Please refer to the accompanying video for the visualization of this experiment.*

[4] M. M. S. Mousavi, G. De Pasquale, A. Somà, and E. Brusa. A novel su-8 microgripper with external actuator for biological cells manipulation. In *Proc. Symp. on Design, Test, Integration & Packaging of MEMS and MOEMS*, pages 356–361, 2011.

[5] F. Hansen, P. Mangell, B. Sonesson, and T. Lanne. Diameter and compliance in the human common carotid arteryvariations with age and sex. *Ultrasound in Medicine & Biology*, 21(1):1–9, 1995.

[6] F. Beyeler, A. Neild, S. Oberti, D. J. Bell, Y. Sun, J. Dual, and B. J. Nelson. Monolithically fabricated microgripper with integrated force sensor for manipulating microobjects and biological cells aligned in an ultrasonic field. *J. of Microelectromechanical Systems*, 16(1):7–15, 2007.

[7] C. Pacchierotti, S. Scheggi, D. Prattichizzo, and S. Misra. Haptic feedback for microrobotics applications: A review. *Frontiers in Robotics and AI*, 3:53, 2016.

[8] F. Ongaro, C. Yoon, F. van den Brink, M. Abayazid, S. H. Oh, D. H. Gracias, and S. Misra. Control of soft untethered grippers for pick-and-place tasks. In *Proc. IEEE RAS/EMBS Int. Conf. on Biomedical Robotics and Biomechatronics*, pages 299–304, 2016.

[9] S. Scheggi, C. Yoon, D. H. Gracias, and S. Misra. Model-based tracking of miniaturized grippers using particle swarm optimization. In *Proc. IEEE/RSJ Int. Conf. on Intelligent Robotic Systems*, pages 454–459, 2016.

[10] F. Ongaro, S. Scheggi, C. Yoon, F. van den Brink, S. H. Oh, D. H. Gracias, and S. Misra. Autonomous planning and control of soft untethered grippers in unstructured environments. *J. of Micro-Bio Robotics*, In Press, 2016.

[11] S. Martel, O. Felfoul, J.-B. Mathieu, A. Chanu, S. Tamaz, M. Mohammadi, M. Mankiewicz, and N. Tabatabaei. MRI-based medical nanorobotic platform for the control of magnetic nanoparticles and flagellated bacteria for target interventions in human capillaries. *Int. J. of Robotic Research*, 28(9):1169–1182, 2009.

[12] J.-B. Mathieu and S. Martel. Steering of aggregating magnetic microparticles using propulsion gradients coils in an MRI scanner. *Magnetic Resonance in Medicine*, 63(5):1336–1345, 2010.

[13] B. J. Nelson, I. K. Kaliakatsos, and J. J. Abbott. Microrobots for minimally invasive medicine. *Annual Review of Biomedical Engineering*, 12:55–85, 2010.

[14] M. Evertsson, M. Cinthio, S. Fredriksson, F. Olsson, H. W. Persson, and T. Jansson. Frequency-and phase-sensitive magnetomotive ultrasound imaging of superparamagnetic iron oxide nanoparticles. *IEEE Trans. on Ultrasonics, Ferroelectrics, and Frequency Control*, 60(3):481–491, 2013.

[15] J Weizenecker, B Gleich, J Rahmer, H Dahnke, and J Borgert. Three-dimensional real-time in vivo magnetic particle imaging. *Physics in Medicine and Biology*, 54(5):L1, 2009.

[16] I. S. M. Khalil, P. Ferreira, R. Eleutério, C. L. de Korte, and S. Misra. Magnetic-based closed-loop control of paramagnetic microparticles using ultrasound feedback. In *Proc. IEEE Int. Conf. on Robotics and Automation*, pages 3807–3812, 2014.

[17] A. Sanchez, V. Magdanz, O. G. Schmidt, and S. Misra. Magnetic control of self-propelled microjets under ultrasound image guidance. In *Proc. IEEE RAS/EMBS Int. Conf. on Biomedical Robotics and Biomechatronics*, pages 169–174, 2014.

[18] X. Wang, X. Ma, and E. Grimson. Unsupervised activity perception in crowded and complicated scenes using hierarchical bayesian models. *IEEE Trans. on Pattern Analysis and Machine Intelligence*, 31:539–555, 2009.

[19] C. Qian, X. Sun, Y. Wei, X. Tang, and J. Sun. Realtime and robust hand tracking from depth. In *Proc. IEEE Int. Conf. on Computer Vision and Pattern Recognition*, pages 1106–1113, 2014.

[20] C. Pacchierotti, F. Ongaro, F. van den Brink, C. Yoon, D. Prattichizzo, D. H. Gracias, and S. Misra. Steering and control of miniaturized untethered soft magnetic grippers with haptic assistance. *IEEE Trans. on Automation Science and Engineering*, In Press, 2017.

[21] D. Jiles. *Introduction to magnetism and magnetic materials*. CRC press, 2015.

[22] T. H. Boyer et al. The force on a magnetic dipole. *American Journal of Physics*, 56(8):688–692, 1988.

[23] I. S. M. Khalil, M. P. Pichel, L. Abelmann, and S. Misra. Closed-loop control of magnetotactic bacteria. *Int. J. of Robotic Research*, 32(6):637–649, 2013.

[24] F. Ongaro, C. Pacchierotti, C. Yoon, D. Prattichizzo, D. H. Gracias, and S. Misra. Evaluation of electromagnetic system with haptic feedback for control of untethered, soft grippers affected by disturbances. In *Proc. IEEE RAS/EMBS Int. Conf. on Biomedical Robotics and Biomechatronics*, pages 908–913, 2016.

[25] J. C. Breger, C. Yoon, R. Xiao, H. R. Kwag, M. O. Wang, J. P. Fisher, T. D. Nguyen, and D. H. Gracias. Self-folding thermo-magnetically responsive soft microgrippers. *ACS Applied Materials & Interfaces*, 7(5):3398–3405, 2015.

[26] J. Van Den Berg, P. Abbeel, and K. Goldberg. Lqg-mp: Optimized path planning for robots with motion uncertainty and imperfect state information. *Int. J. of Robotic Research*, 30(7):895–913, 2011.

[27] S. Patil, J. Van Den Berg, and R. Alterovitz. Estimating probability of collision for safe motion planning under gaussian motion and sensing uncertainty. In *IEEE Int. Conf. on Robotics and Automation*, pages 3238–3244, 2012.

[28] S. M. Lavalle. Rapidly-exploring random trees: A new tool for path planning. Technical report, Computer Science Dept., Iowa State University, 1998.

[29] E. Gultepe, J. S. Randhawa, S. Kadam, S. Yamanakaand F. M. Selaru, E. J. Shin, A. N. Kalloo, and D. H. Gracias. Biopsy with thermally-responsive untethered microtools. *Advanced materials*, 25(4):514–519, 2013.